Available online at www.sciencedirect.com
SCIENCE DIRECT
Biomedical Signal Processing and Control 1 (2006) 64–77
Biomedical Signal Processing and Control
www.elsevier.com/locate/bspc

A Data mining framework of noninvasive intracranial pressure assessment

Xiao Hu *, Valeriy Nenov, Marvin Bergsneider, Neil Martin

Division of Neurosurgery, Geffen School of Medicine at University of California, Los Angeles, CA 90095, United States

Received 29 November 2005; received in revised form 5 May 2006; accepted 11 May 2006

Abstract

The only established technique for intracranial pressure (ICP) measurement is an invasive direct procedure that has been accepted into routine usage in neurosurgical services. However, there are many other scenarios where a noninvasive assessment of ICP is highly desirable. To make a full use of the vast amount of signals collected in a typical neurosurgical service environment to realize such a noninvasive procedure of ICP assessment, a general data mining framework is proposed in the present work. As a particular implementation of the proposed framework where continuous arterial blood pressure (ABP) and cerebral blood flow velocity (CBFV) are available, we propose to simulate the unobserved ICP as the output of a model built from a database composed of arterial blood pressure, cerebral blood flow velocity and ICP. This model was discovered by exploring the database with the hemodynamic features extracted from measured ABP and CBFV. This approach was evaluated using a database composed of 30-min long measurements from nine traumatic brain injury patients. The approach achieved significant improvements of ICP simulation accuracy over several existing noninvasive ICP assessment methods. Particularly, its median normalized prediction error for ICP is 39% compared to 51% as obtained by an existing method and its median correlation coefficient between estimated and measured normalized ICP is 0.80 compared to 0.35 achieved by the existing method. The proposed framework is flexible in incorporating other relevant signals besides ABP, CBFV and ICP into the database. It allows for designing new hemodynamic feature vectors and for adopting new models for ICP estimation. Hence it is worthwhile to evaluate the method using a larger database and further develop the framework.

Keywords: Noninvasive; Intracranial pressure; Data mining; System identification

1. Introduction

Although several noninvasive techniques of measuring intracranial pressure (ICP) have been proposed during the last decade [1–5], the only established means of intracranial pressure measurement is an invasive direct procedure, which accesses the intracranial space in ventricles, parenchymal, or epidural space for sensing ICP. Albeit this invasiveness, long term monitoring of ICP has been part of established protocols of managing brain injury patients in a neurosurgical intensive care unit. The risk involved in an invasive ICP measurement is justified in such a critical scenario because of the demonstrated benefits of outcome improvement of brain injury patients. However, there are many other situations where an assessment of ICP, or even a monitoring, is desirable but an invasive procedure is inappropriate. For instance, these situations may include: management of fulminant hepatic failure (FHF) and liver transplant patients where ICP monitoring allows a specific therapy to control intracranial hypertension but is especially risky for patients with coagulopathy [6]; in a non-specialized units where the ICP sensor placement is not possible [7]; management of normal pregnant women or those with pre-eclampsia [8]. Furthermore, even in a neurosurgical setting, noninvasive ICP is highly desirable follow-up assessment of hydrocephalous patients with implanted shunts.

In addition to the attempts of realizing noninvasive ICP (NICP) by avoiding invasively penetrating the intracranial space by measuring skull displacement, by MR imaging of CSF dynamics, and by measuring inner ear pressure, etc., a large amount of research has been conduced on using transcranial doppler (TCD) ultrasound for a NICP assessment. The first

* Corresponding author. Tel.: +1 310 825 4346.
E-mail addresses: xhu@mednet.ucla.edu (X. Hu), vnenov@mednet.ucla.edu (V. Nenov), mbergsneider@mednet.ucla.edu (M. Bergsneider), nmartin@mednet.ucla.edu (N. Martin).

1746-8094/$ – see front matter
doi:10.1016/j.bspc.2006.05.003

proposal of such a method might be attributed to Aaslid et. al. [9] about a decade ago. A simple formula, which relates arterial blood pressure and cerebral blood flow velocity (FV) to cerebral perfusion pressure(CPP), was proposed. CPP for cerebral vascular bed has been operationally defined as the difference between arterial blood pressure (ABP) and ICP and hence intimately associated with ICP. The motivation behind this proposal is that changes in ICP will cause secondary changes in pressure-flow characteristics of the cerebral vascular bed. Besides the original Aaslid formula, several extensions have been reported [10,11], most of which replaced the calculation of the first harmonics of flow velocity and blood pressure in the original formula with some more readily calculable time domain parameters such as peak systolic and end diastolic values.

The observation that changes of FV of basal arteries, cerebral sinus, and veins follow ICP changes is abundant in literature. It is a well known phenomenon that ICP elevation can lead to a decline in end-diastolic FV [12]. The correlation between ICP and derived indices from FV waveforms such as pulsatility index (PI) [13], resistance index (RI) [13], and trans systolic time (TST) [13] has been well studied in various ICP conditions.

The experimentally observed interdependency between TCD FV and ICP signals is just a manifestation of the inherent coupling between the cerebral hemodynamic system and intracranial cerebrospinal fluid (CSF) dynamic system from which FV and ICP are two observed variables. This can be illustrated using some well known multi-compartmental intracranial dynamic models [14–16]. In Ursino's models, ICP is usually one of state variables of the dynamic system while CBFV is an instantaneous function of several state variables. As a particular example, state variables may include pressures at various compartments and the autoregulation factor of the proximal cerebral vascular bed in the model [17]. Due to the evolution of the state variables in a coupled fashion, CBFV as a function of some state variables may carry information about ICP as confirmed by various experimental observations.

Given the complex interaction between cerebral vascular bed and intracranial dynamics, NICP assessment using formula based methods is probably overly simplistic. Furthermore, these formula based methods cannot produce a continuous ICP waveform and cannot give an assessment of the quality of the estimate. On the other hand, the complexity of the system might impede an accurate mathematical description of it, and in consequence, poses a great challenge to the application of a well known hidden state estimation algorithm, i.e., the Kalman filter [18] to perform NICP even though the NICP assessment using TCD can be well posed as a problem of state estimation from noisy measurements. As an enhancement to the formula based methods as well as an alternative to the model-based state estimation filters, a series of data-driven methods due to Czosnyka et al. has been proposed [19–21]. The fundamental difference between these methods and the formula based ones is that the latter only uses ABP and TCD FV signals from the patient for whom NICP is to be assessed while the former explores a database of signals that may be from different patients. This is indeed a promising direction. The existing implementation of this data driven method relies on deriving a fixed linear mapping from so called TCD characteristics to coefficients of a finite impulse response (FIR) filter that takes an ABP signal as input and simulates an ICP output. However, there are several limitations in this implementation. First of all, it has a rigid structure in the sense that TCD characteristics are directly mapped to coefficients of an ABP $\rightarrow$ ICP model. This choice first limits the model to those that can be expressed in terms of a small number of coefficients. This excludes lots of useful models such as linear models in a state space form, nonlinear models, and local linear models. Furthermore, if different models other than a FIR filter are to be used, the mapping function has to be re-trained. Secondly, adding new data to the database cannot guarantee the improvement of the performance or even preserve the performance achieved before expanding database. A new entry in the database will cause the global mapping function to be changed in a profound fashion resulting in an unpredictable behavior of the whole system. Thirdly, the quality of estimated ICP cannot be assessed and one has to simply take whatever simulator provides without any clue of whether it is a good estimate or not.

The present work aims at proposing an improved framework for data mining cerebral hemodynamic signals for NICP assessment that avoids all the limitations mentioned above. The framework comprises two major parts: a trainer and a simulator. The trainer is to explore the existing knowledge in signal database and organize it into a mapping function by which the database becomes searchable. The simulator first constructs a hemodynamic feature vector from ABP and CBFV that can be used as the input to the mapping function for querying the database. The query will return the most suitable record that can be used for building an ICP estimation model on the fly. The simulator then simulates this model to obtain unobserved ICP.

The above description serves as a conceptual summary of the framework. Section 2 will be devoted to its concretization. Specifically, a more detailed description of each block of the framework will be provided in Section 2.1. Then their implementations will be introduced in subsequent subsections. In Section 3, the validation results of several implementations will be shown and discussed in Section 4.

2. Methods

2.1. Introduction of the framework

Block diagrams are presented in Figs. 1 and 2 for the trainer and the simulator respectively. As shown in these diagrams, the core of the proposed approach is a signal database that is collection of ABP, CBFV, invasive ICP signals, and other relevant signals (e.g. PCo_2, ECG, etc.). A simultaneous record of them will be stored as a database entry. Length of each entry should be long enough to facilitate the extraction of low frequency information. It should also be short enough to be reasonably treated as generated from a dynamic system with constant parameters.

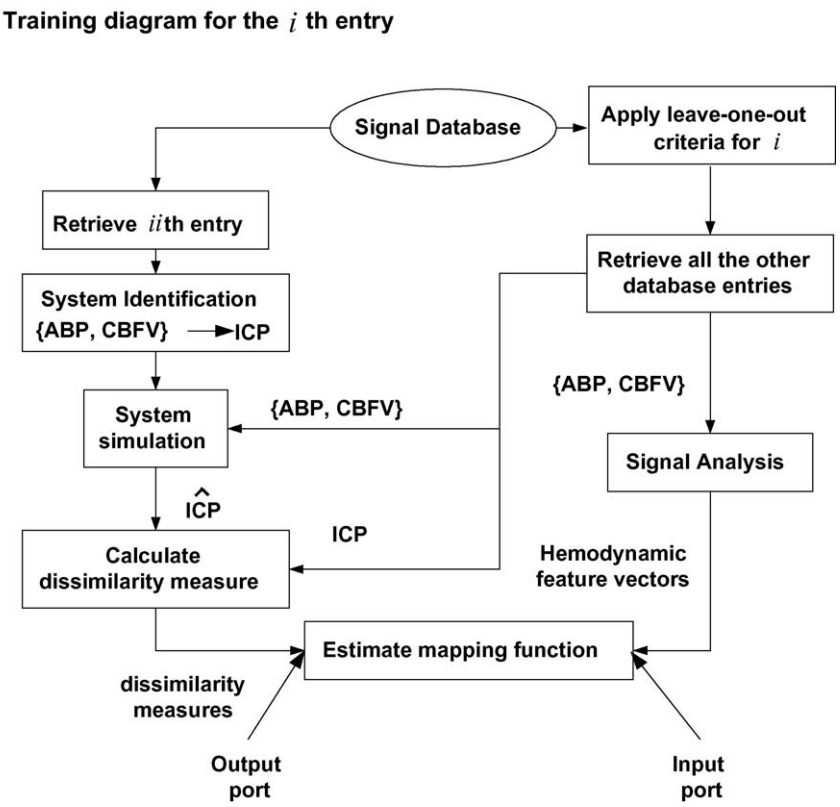

Fig. 1. Training diagram of the proposed noninvasive intracranial pressure estimation framework. ABP stands for arterial blood pressure; CBFV for cerebral blood flow velocity; ICP for intracranial pressure. Each entry in database may contain a segment of simultaneously recorded ABP, CBFV, and ICP. Furthermore, other relevant signals like PCO_2 may be incorporated into database entries. Hemodynamic feature should be extracted from signals excluding ICP.

Another central piece in both diagrams is the mapping function. The establishment of the mapping function occurs in the training phase where each entry in the database will be associated with one mapping function. This mapping function takes a hemodynamic feature vector as its input and outputs a dissimilarity measure. Consequently, it predicts how well the model built from this entry will perform in simulating ICP for signals whose hemodynamic feature vectors are input to the mapping function.

The signal analysis block in both diagrams represents a procedure applied to signals excluding ICP for extracting a hemodynamic feature. As discussed in Section 1, the proposed method is built upon the central premise that the cerebral hemodynamics is under the influence of the CSF dynamics and thus a suitable hemodynamic feature might carry information that could be used as a probe to the CSF dynamics. In light of this, the designed hemodynamic features should be able to characterize the unique aspect of hemodynamic state that can be attributed to the effect of CSF dynamics.

System identification generally refers to the process that builds a model directly from a given set of input–output data [22]. In this framework, such a model is used for simulating ICP. Hence, ABP and CBFV are treated as input and ICP as output to the model. Choices of appropriate system identification methods and ICP simulation models are independent from rest of the blocks in the framework. A

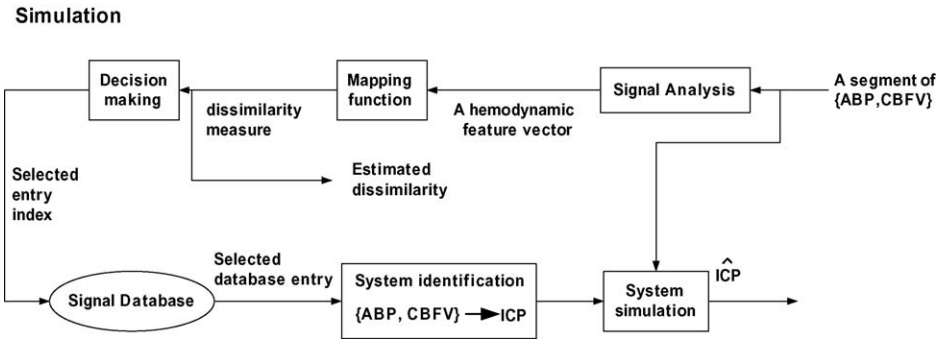

Fig. 2. Simulation diagram of the proposed noninvasive intracranial pressure estimation framework. The mapping function shown in the block diagram is to be obtained from the training process shown in Fig. 1.

greater flexibility has been introduced into the framework by this modularization.

Dissimilarity measures the distance between simulated and measured ICP for a given criterion. Having the mapping function output different types of dissimilarity measures makes the resultant NICP close to a particular aspect of ICP. This flexibility is highly desirable. As is well known, there are several components in ICP, which may suite different clinical purposes. For example, mean ICP is still the most clinically relevant parameter that affects many clinical decisions. Pulsatile ICP has been proposed to characterize intracranial compliance [23]. On the other hand, slow waves in ICP might provide autoregulation status of the cerebral vascular bed [24]. The adoption of different dissimilarity measures also embodies the strategy of 'divide and conquer' meaning that simulating different aspects of ICP separately can result in a complete ICP assessment.

Flexibility of accommodating different implementations also exists in the decision making block. Based on the outputs of each mapping function, decision has to be made as to which database entry should be selected for building the model. The simplest one would be just selecting the one having the smallest predicted dissimilarity. In addition to this simple-minded decision, high level information regarding the database entries can also be incorporated. Such high level information may include clinical symptoms and observations of the patients, and the temporal closeness of two database entries. Furthermore, statistical information of the mapping function output such as its variance can also be explored to build a more robust statistical decision maker.

A description of each block's functionality as well as its interactions with others has been presented in this subsection. In sequel, exemplary implementations of the proposed framework will be introduced.

2.2. Signal database

The present implementation of the proposed framework relies on a database of nine traumatic brain injury patients. Each patient has a 30-min long passive recording of ABP, ICP and CBFV. CBFV was obtained at the right middle cerebral artery, ipsilateral to the ICP measurement location, with ultrasonography transducers fixed to a headband to prevent motion artifacts. CBFV at left middle cerebral artery was not used in this study. ABP was measured through radial arterial-lines while ICP was measured using ventricular catheter connected to an external strain gauge. All three signals were fed into GE bedside multi-modality monitors, which were then simultaneously sampled at 75 Hz using an in-house data acquisition system equipped with proper interfaces to the bedside patient monitors. This data set was part of the data collected in a previous study of using hyperventilation and metabolism therapy methods in controlling ICP [25]. The criterion for selecting the nine patients in the present study is that their archived data included continuous measurements of ABP, ICP and CBFV signals, a prerequisite for the proposed noninvasive ICP assessment approach. This study was conducted with proper internal review board (IRB) approval. Informed consents for the study were obtained from patients or their relatives at appropriate situations. As a summary, key patient characteristics were listed in Table 1.

Each 30-min long data segment was decomposed into 20 consecutive short segments, each of which contains about 100 heart beats of data. This segment length was chosen as a compromise between the requirements of capturing long-term changes in signals and being able to treat such a segment as from a constant-parameter dynamic system.

2.3. Hemodynamic features

In this study, we have explored several ways of constructing hemodynamic features from measurements of ABP and CBFV, each of which will be introduced.

2.3.1. Slow wave dynamics

Slow wave components having a frequency below heart rate have been identified in ABP, CBFV, and ICP in previous studies [26–28]. They may have different physiological origins and interact with each other in a non-trivial fashion. Of interest here is that slow waves in CBFV carry information regarding how the cerebral vascular bed responses to the slow waves present in ABP and ICP.

Table 1
Key Patient Characteristics

	A	G	D	GCS	GOS_3	GOS_12	PID	ABP	CBFV	ICP
1	58	M	Left frontal SDH	8	3	6	3	101.2 ± 22.8	77.1 ± 20.0	12.5 ± 2.3
2	57	F	Left frontal SAH	6	3	3	1	126.1 ± 38.5	132.6 ± 49.6	12.9 ± 3.7
3	68	M	Brain Stem injury	4	Dead		3	92.3 ± 23.2	50.7 ± 14.3	23.5 ± 5.7
4	59	F	Left frontal contusions	8	3	5	6	132.8 ± 35.6	71.0 ± 20.4	15.3 ± 4.3
5	25	M	SAH	6	3	5	1	117.1 ± 17.9	27.8 ± 5.8	15.1 ± 3.9
6	29	M	SAH in left sylvian fissure	3	8	7	1	92.3 ± 19.8	42.8 ± 22.1	24.3 ± 5.3
7	47	M	Bilateral frontal IAH	7	3	3	1	81.7 ± 20.1	54.0 ± 17.3	8.8 ± 4.1
8	21	M	Basal ganglia punctate hemorrhage	7	3	3	3	132.6 ± 25.0	94.1 ± 15.1	11.7 ± 0.2
9								74.8 ± 22.1	29.1 ± 19.0	9.6 ± 0.3

A—age in years at injury; G—gender; D—diagnostic description; GCS—Glasgow Coma Scale at measurement [40]; $GOSE_3$—3 month Glasgow Outcome Score extended [41]; $GOSE_{12}$—12 month Glasgow Outcome Score extended; PID—post-injury day at measurement; ABP—arterial blood pressure (mmHg); CBFV—cerebral blood flow velocity at MCA (cm/s); ICP–intracranial pressure (mmHg); SAH—subarachnoid hemorrhage; SDH—subdural hematoma; IAH—intracerebral hemorrhage.

To extract the slow wave component, beat-to-beat average of corresponding signal was first extracted and resampled, using a cubic spline, at 2 Hz. Each beat was delineated using ABP waveform and the results were visually checked. To extract a hemodynamic feature vector from these signals, a linear autoregressive model with exogenous input (ARX) was fitted to the output/input pair of CBFV/ABP and the resultant model coefficients used as hemodynamic feature vectors. A linear dynamic system has been considered adequate for modeling the input/output relationship between slow waves of ABP and CBFV [29] that were extracted in the similar way. Model orders were determined as the median of optimal model orders found for all signal entries. Minimum description length (MDL) criterion was adopted for determining optimal order for each entry. For an easy reference, the hemodynamic feature thus created is denoted as F_{slow}.

2.3.2. Waveform analysis

By resorting to waveform analysis, the following measures were extracted in a beat-to-beat fashion including trans systolic time [13], resistance area product (RAP), critical closing pressure (CCP) [30], CBFV pulsatility index [13], resistance index [13], mean FV (mFV), amplitude of FV (pFV), systolic FV (sFV) and diastolic FV (dFV).

This procedure resulted in a beat-to-beat time series for each measure. We derived two types of hemodynamic features from these time series. The first type was static in the sense that mean and standard deviation of the each time series were cascaded into a hemodynamic feature denoted as (F_{sta}). On the other hand, to derive the second type of hemodynamic feature, an autoregressive model (AR) was fitted to each secondary time series and the model coefficients were cascaded into a hemodynamic feature designated as (F_{dyn}). The AR model order was determined using the same procedure.

2.3.3. Full dynamics

In contrast to the procedures mentioned above where slow wave components extracted from original signals were used for feature extraction, a full dynamic feature was constructed based on raw waveforms. Specifically, an ARX model was adopted again but with a higher model order to fit each CBFV and ABP pair. Two kinds of feature vectors were then derived from the model coefficients. As known from system theory, two transfer functions for two outputs of a linear dynamic system with the same input should share a common denominator, which determines the inherent system properties such as resonant frequencies. In the present context, the coupled cerebral hemodynamic and intracranial hydraulic systems can be treated as one system with ABP as its input and CBFV and ICP as its output. Thus, the feature vector composed solely of the ARX denominator coefficients should be a better characterization of the properties of the combined system by excluding what is specific to the ABP → CBFV transfer function. This feature vector was denoted as F_{den}. As a comparison, a second feature denoted as F_{full} composed of all the model coefficients was also included.

2.3.4. Feature selection

One important property of various feature vectors is their separability in the feature space. For pattern classification purposes, a feature set with good separability is desirable. In this NICP assessment context, separability might have to be treated differently because the hemodynamic features extracted here are to be used as the input to a continuous mapping function. Due to this requirement of continuity, if the feature vectors in the training set are well separated, it will be harder to obtain a continuous mapping function from such a disjoined data set.

To investigate this issue, we used the same technique applied in our previous study [31] to analyze the structure of high dimensional feature vectors. Specifically, each patient becomes a class. A class-independent linear discriminate analysis (LDA) was performed to reduce the dimension of the original feature vector for the purpose of visualization as well as to quantify its inter-patient separability. This was achieved by solving the following generalized eigenvalue decomposition

$$S_{\text{b}} a_i = \lambda_i S_{\text{w}} a_i, \quad \lambda_1 \geq \lambda_2 \geq \ldots \geq \lambda_m \tag{1}$$

where S_{b} is the between-class covariance matrix of the hemodynamic features, S_{w} the within-class covariance matrix, and λ_i is the ith eigenvector. m is the dimension of the original feature space. a_i s are the generalized eigenvectors. The leading three of them also give the directions of the subspace where the original feature will be projected onto for visualization. λ_i is positively proportional to the degree of separability of the features along a_i, thus different feature sets' separability can be compared based on λ_i s. S_{b} and S_{w} can be obtained in the usual way as found in [31].

2.4. System identification

There are a large number of classes of dynamic models, including both discrete-time and continuous-time, linear and nonlinear ones, that can be used for simulating ICP given ABP and CBFV as input. Only serving as an illustration in the present work, a discrete linear dynamic system is explored here. Particularly, a stable deterministic linear dynamic model was used to represent the input/output relationship between ABP, CBFV and ICP. Its identification was conducted using the subspace identification method [32]. This algorithm is able to identify, given input/output data, the following state space model

$$\begin{aligned} x_{n+1} &= Ax_n + Bu_n + w_n \\ y_n &= Cx_n + Du_n + v_n \end{aligned} \tag{2}$$

with

$$E\left[\begin{pmatrix} w_p \\ v_p \end{pmatrix} \begin{pmatrix} w_k & v_k \end{pmatrix}\right] = \begin{pmatrix} Q & S \\ S^T & R \end{pmatrix} \delta_{pk} \tag{3}$$

where A, B, C, and D are system matrices to be identified, y_n is the model output at time n, i.e, ICP, and u_n is the model input including ABP and CBFV. w_n and v_n are zero-mean, stationary Gaussian white noise series, hence $\delta_{pk} = 0$ if $p \neq k$. They are termed state noise and observation noise, respectively. The key of subspace identification algorithm is the proof that unknown state

variable x_n as well as its dimension can be estimated from block Hankel matrices formed from the input and output data. With estimated x_n available, remaining matrices A, B, C, D, Q, S, and R can be estimated using the well established linear least squares method. Therefore, two major steps of a subspace identification include: (1) estimation of model dimension and sequence of x_n, usually by projecting the row space of data block Hankel matrices and then applying singular value decomposition; (2) solve a least squares problem to obtain unknown model matrices. Three major variants of subspace algorithm exist that include multivariable output-error state space(MOSEP) [33], canonical variate analysis(CVA) [34], and numerical algorithms for subspace state space system identification (N4SID) [32]. The implementation of the subspace algorithm in the System Identification Toolbox found in Matlab 7.0 was used in the present work. This implementation contains automatic procedures of selecting prediction horizon based on akaike information criterion (AIC), selecting either MOSEP or CVA algorithm, and determining model dimension based on SVD. Details of this implementation can be found in the text book [22].

2.5. Dissimilarity measures

The following five types of dissimilarity measures were investigated, each of which tries to match simulated ICP with unobserved ICP in a particular aspect.

The first metric is defined as:

$$e^{(1)} = \frac{1}{N} \frac{\sum_{i=1}^{N} |y_i - \hat{y}_i|}{|\bar{y}|}. \tag{4}$$

where N is number of samples, y_i is the ith sample of unobserved ICP waveform and $\hat{y}_i$ its corresponding estimate. $e^{(1)}$ calculates the mean absolute error between a signal y and its estimate $\hat{y}$ normalized by the mean of signal $\bar{y}$. This is a comprehensive metric in the sense that both the mean value and waveform shape of $\hat{y}$ have to be close to those of y in order to achieve a small $e^{(1)}$.

The second metric is defined as:

$$e^{(2)} = \frac{|\bar{\hat{y}} - \bar{y}|}{|\bar{y}|} \tag{5}$$

It calculates the normalized absolute error between the mean estimated ICP and the mean original ICP. This is motivated because the mean ICP is still the most used information for clinicians in which case the shape of the waveform might not be a concern.

The third metric is defined as:

$$e^{(3)} = 1 - \mathrm{corr}(y^N, \hat{y}^N), \tag{6}$$

which lies in the range $[0, 2]$. $\mathrm{corr}(x, y)$ is the operator for calculating the zero-lag cross correlation coefficient between x and y. This metric excludes the effect of mean signal level and puts more emphasis on the matching of the two signals in their general trend. To calculate $e^{(3)}$, it was found advantageous to derive $\hat{\mathrm{ICP}}$ using normalized ABP and CBFV in both model identification and simulation phase. Thus, y^N stands for the normalized ICP and $\hat{y}^N$ its estimate. The normalization of a signal x was carried out as

$$x^N = \frac{x - \bar{x}}{\bar{x}} \tag{7}$$

The fourth metric is defined as:

$$e^{(4)} = \frac{\sum_{i=1}^{N} |y_i^{\mathrm{P}} - \hat{y}_i^{\mathrm{P}}|}{N|y^{\mathrm{P}}|}. \tag{8}$$

where y^{P} represents the pulsatile component of signal y and $|y^{\mathrm{P}}|$ denotes the average amplitude of the pulse. Hence, this measure emphases matching the pulsatile component. As for deriving $e^{(3)}$, $\mathrm{ICP}^{\mathrm{P}}$'s estimate was derived by using corresponding pulsatile components of ABP and CBFV for model identification and simulation. Understandably, such models were different from those used in calculating $e^{(3)}$, which were built using normalized signals.

To match the slow wave components, we propose the fifth metric as:

$$e^{(5)} = \frac{\sum_{i=1}^{N} |y_i^{\mathrm{S}} - \hat{y}_i^{\mathrm{S}}|}{N|y^{\mathrm{S}}|} \tag{9}$$

where y^{S} represents the slow-wave component of signal y and $|y^{\mathrm{S}}|$ denotes the mean of y^{S}. Similarly, $\mathrm{I}\,\hat{\mathrm{C}}\,\mathrm{P}^{\mathrm{S}}$ was derived by building and simulating the linear dynamic model using slow wave components of ABP and CBFV.

In summary, there are four different ICP simulation models that have to be identified using the method described in 2.4. To calculate $e^{(1)}$ and $e^{(2)}$, the model will be built using unfiltered ABP, CBFV and ICP; normalized signals will be used to calculate $e^{(3)}$; pulsatile components of signals will be used to calculate $e^{(4)}$; slow-wave components will be used for $e^{(5)}$. This design of various dissimilarity measures reflects possible requirements that a NICP assessment method might have to satisfy. The correlation among those measures are very low by design, hence different ICP simulation models and different mapping functions should be built for them.

2.6. Mapping function

In the present implementation, the input to the mapping function comprises of hemodynamic features. The predicted dissimilarity serves two purposes: (1) guide the database query, i.e., those promising in achieving less simulation error will be returned upon query; (2) provide an estimate of the final quality of the NICP simulation.

The first step to obtain such a mapping function is to perform a complete cross validation of the database entries. Suppose there are N entries in the database. First, an ICP simulation model is built for each entry resulting in N models. Second, the ith model is used to simulate ICP and compute a dissimilarity measure (as defined above) for each database entry. Repeating this step for all the entries in the database will result in a dissimilarity matrix $E_{N\times N}$, the ith row of which are dissimilarities between the ith model simulated ICP and the measured ICP of all the data entries. This row vector thus serves

as the output of the training data set to learn the mapping function for the ith data entry.

There is no prior information about the appropriate form that this mapping function should be. It is also understandable that it might depend on different hemodynamic features as well. Ideally, a flexible function approximator like multi-layer feed forward neural network is a good choice. However, a practical problem we encountered was that the amount of available training data did not match well with the number of unknown parameters in a useful neural network. To train each mapping function, the number of training input–output pairs is 160 because the 20 data entries associated with the corresponding patient whose associated mapping functions are being trained should be excluded for a realistic testing of the performance of the method. On the other hand, the smallest hemodynamic feature F_{slow} has a dimension of 4. Following a typical recommendation of a two layer network configuration [35], the number of hidden units at each hidden layer would be 8 and 4. This choice will result in 80 unknown network weights and biases. There will be a great probability of overfitting the network to learn these 80 unknown with 160 input–output pairs. Taking this into consideration, a linear function was selected to predict dissimilarity e given hemodynamic feature vectors F such that

$$e = F^{\mathrm{T}} b \tag{10}$$

where e is a scalar representing the dissimilarity output, F is a column hemodynamic vector, and b is a column coefficients vector having the same dimension as F. Given the training data set, which contains e_i and F_i with $i = 1, \ldots, N_k$, application of a linear least squares estimation results in an estimate of b as

$$\hat{b} = \left(\mathbf{F}^{\mathrm{T}}\mathbf{F}\right)^{-1}\mathbf{F}^{\mathrm{T}}\mathbf{e} \tag{11}$$

where N_k is the total number of database entries minus the number of excluded ones and $\mathbf{F}$ is a $N_k \times d$ data matrix, ith row of which is F_i^{T}. $\mathbf{e}$ is a column vector comprised of e_i. Standard linear regression theory tells that the covariance of the $\hat{b}$ is

$$V_b = \left(\mathbf{F}^{\mathrm{T}}\mathbf{F}\right)^{-1}\sigma^2 \tag{12}$$

where σ^2 is the variance of the observational noise present in $\mathbf{e}$, which is usually assumed to be white Gaussian noise. This assumption leads to the result that $\hat{b}$ is normally distributed with its mean being the unknown b and its covariance matrix being V_b. It will be shown that a statistical query can be designed based on this result.

2.7. Query database

A hemodynamic feature is used to query the database with an additional specification of the dissimilarity measure to be used. Internally, it will be fed into the appropriate mapping function associated with each database record. Based on mapping functions' output e_i, $i = 1, \ldots, n$, a decision has to be made with regard to which entry is to be returned in response to the query. We investigated two implementations of such a process. The first was a deterministic winer-takes-all approach, which returns the database entry having the smallest predicted dissimilarity measure. The second one was a statistical decision maker. $\hat{b}$ is a random variable and normally distributed with the true b being its expectation and V_b its covariance matrix. Hence, the output of a mapping function $e_i = F_i^{\mathrm{T}}\hat{b}$ is also a normal random variable with its mean being the true mapping function output $F_i^T b$ and its variance being $F_i^{\mathrm{T}} V_b F_i$. Furthermore, we assume that outputs from different mapping functions are independent. This leads to the conclusion that the variable $e_i - e_j$, $i \neq j$ is also normally distributed with $F_i^{\mathrm{T}} b - F_j^{\mathrm{T}} b$ being its mean and $F_i^{\mathrm{T}} V_b F_i + F_j^{\mathrm{T}} V_b F_j$ being its variance. With this result, the standard z value for testing the difference between e_i and e_j can be computed as

$$z_{i,j} = \frac{e_i - e_j}{\sqrt{F_i^{\mathrm{T}} V_b F_i + F_j^{\mathrm{T}} V_b F_j}}. \tag{13}$$

To proceed, a score will be assigned to e_i as the number of positive hypothesis test that e_i is smaller than e_j, $j = 1, \ldots, n$ using $z_{i,j}$. Consequently, the entry that achieves the maximal score will be selected.

2.8. Method validation

The validation was carried out using the leave-one-patient-out schema. To proceed, the mapping function will be trained using the data from eight patients and tested on the remaining one.

As comparisons to the proposed method, we implemented the following published NICP methods for assessing mean ICP:

- Aaslid's original proposal

$$\hat{\mathrm{ICP}}_{\mathrm{m}} = \mathrm{ABP}_{\mathrm{m}} - \frac{\mathrm{CBFV}_{\mathrm{m}}|\mathrm{ABP}_1|}{|\mathrm{CBFV}_1|} \tag{14}$$

- Czosnyka method

$$\hat{\mathrm{ICP}}_{\mathrm{m}} = \mathrm{ABP}_{\mathrm{m}} - \frac{\mathrm{ABP}_{\mathrm{m}} \times \mathrm{CBFV}_{\mathrm{dias}}}{\mathrm{CBFV}_{\mathrm{m}}} - 14 \tag{15}$$

- Belfort method

$$\hat{\mathrm{ICP}}_{\mathrm{m}} = \mathrm{ABP}_{\mathrm{m}} - \frac{\mathrm{CBFV}_{\mathrm{m}} \times (\mathrm{ABP}_{\mathrm{m}} - \mathrm{ABP}_{\mathrm{dias}})}{\mathrm{CBFV}_{\mathrm{m}} - \mathrm{CBFV}_{\mathrm{dias}}} \tag{16}$$

where $|\mathrm{ABP}_1|$ and $|\mathrm{CBFV}_1|$ represent the amplitudes of the harmonic of ABP and CBFV corresponding to heart rate respectively. $\mathrm{ABP}_{\mathrm{m}}$ stands for the mean ABP and $\mathrm{ABP}_{\mathrm{dias}}$ for the diastolic ABP. The same notation applies to CBFV as well.

In addition, the method due to Schmidt and Czosnyka et al [19] capable of assessing ICP waveform has also been implemented and compared to the proposed data mining approach. A modified version [21] of this method has been published. However, it needs two well-defined signal databases that contain signals from a patient population with preserved pressure autoregulation and those from a patient population with impaired pressure autoregulation, respectively. To construct such database would need significantly more patients

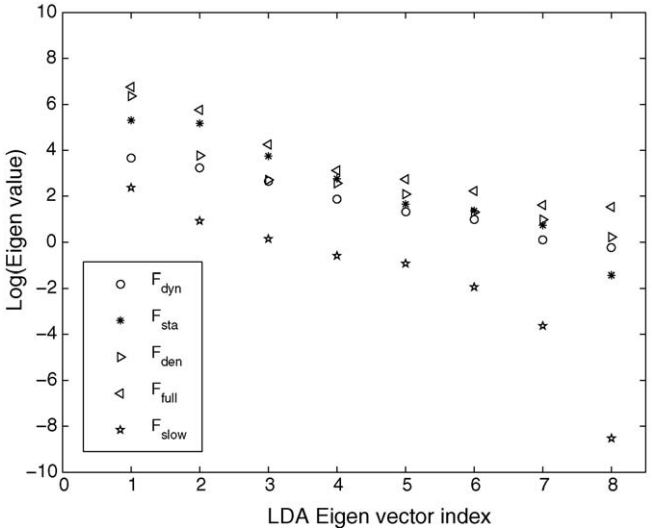

Fig. 3. Logarithm of the linear discriminant analysis eigenvalues of the five types of hemodynamic features investigated in the paper. Eigenvalues of each feature type are positively proportional to the separability of the feature along the corresponding eigenvectors' directions.

than what were available to this study. In addition, the increased complexity would make a faithful implementation of this modified method less possible. Therefore, we chose to implement the original version of the method for comparison.

3. Results

Hemodynamic feature F_{slow} was extracted from ARX model coefficients. The order was determined to be $(6, 2)$ for denominator and numerator polynomials of the transfer function, respectively. F_{dyn} was extracted from nine AR models. The order of each model was determined as 4. F_{full} and F_{den} were extracted from an ARX model with orders (8, 24).

3.1. Hemodynamic features

LDA eigenvalues of five types of hemodynamic features are presented in Fig. 3. F_{slow} has the lowest patient separability while F_{full} is the most discriminant one. As expected, F_{den} is less discriminant than F_{full} since the later contains the former. To test which type of feature will be more appropriate for being used as input to mapping functions, the leave-one-patient-out validation was conducted based on $e^{(5)}$ using F_{full} and F_{slow} as input to the mapping function, respectively. The final $e^{(5)}$ achieved for both of them is presented in Fig. 4. Overall, F_{slow} achieved smaller $e^{(5)}$ except for two data entries from patient No.4. This analysis indicates that hemodynamic features with less inter-patient discriminant ability are preferred as the input to the mapping function. Following this result, the rest of the computations was based on F_{slow}.

3.2. Different query methods

The performance of the deterministic and the statistical query methods is compared in Fig. 5 based on $e^{(2)}$. The statistical query method did improve the robustness of results by suppressing those erroneous ones present for some data segments from patients No. 4 and 5. This observation was also true for other dissimilarity measures. For this reason, the statistical query method is preferred.

3.3. Comparisons to other published methods

Based on the previous results, the best implementation of the proposed framework is to use F_{slow} as the hemodynamic feature vector and the statistical query method for retrieving the appropriate data entry. This implementation was then compared to the three published formulas for estimating mean ICP and the result is shown in Fig. 6 in terms of $e^{(2)}$. Results from

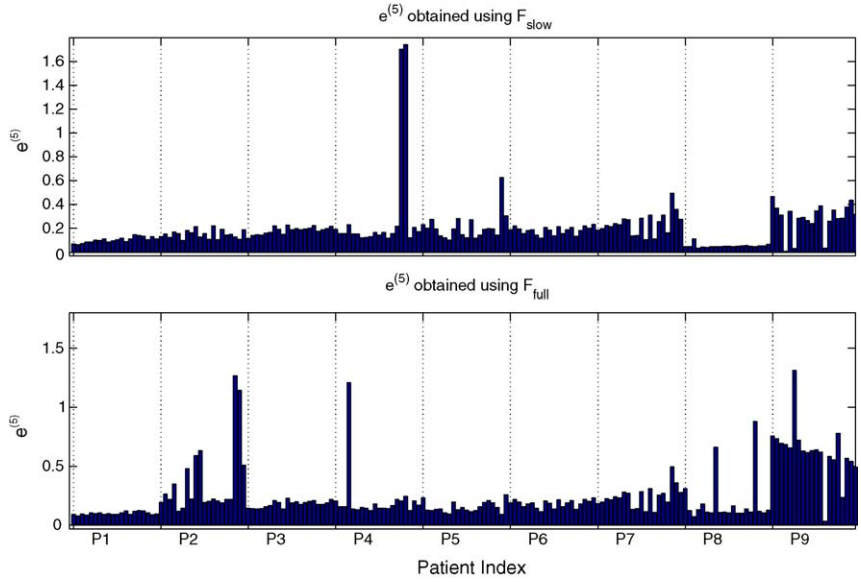

Fig. 4. Comparison of F_{slow} and F_{full} s' performance of NICP assessment based on dissimilarity measure $e^{(5)}$. $e^{(5)}$ was obtained in a leave-one-patient-out fashion using the robust query method.

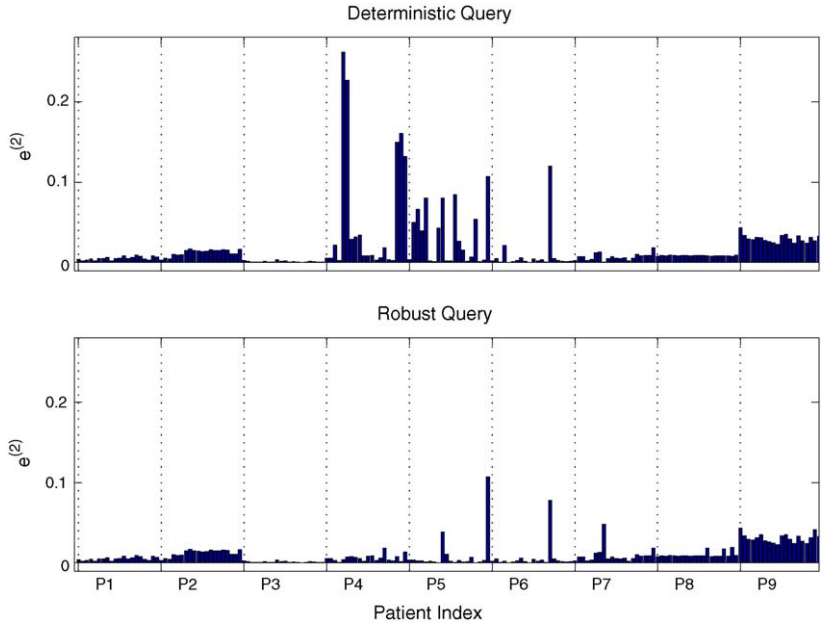

Fig. 5. Comparison of the deterministic and the statistical query methods based on $e^{(2)}$, which was obtained using CBFV as model input.

comparison to the Schmidt's method are presented in Fig. 7 based on $e^{(1)}$, $e^{(3)}$ and $e^{(5)}$. Formula based methods essentially did not work for this nine-patient database because the relative errors are very high while the data mining approach's relative error is in the range of $[0.007\%, 10.1\%]$. The Schmidt's method is capable of simulating ICP waveform. Nevertheless, the results shown here demonstrate that the proposed method outperformed it significantly.

3.4. Waveform of estimated ICP

Fig. 8 gives summary plots of several comparisons between estimated, based on different dissimilarity measure, and measured ICP. Three representative database entries for each of $e^{(3)}$, $e^{(4)}$, and $e^{(5)}$ were shown. They correspond to those entries whose dissimilarity measures are the smallest, closest to the 10 percentile and closest to the 50 percentile, respectively. It

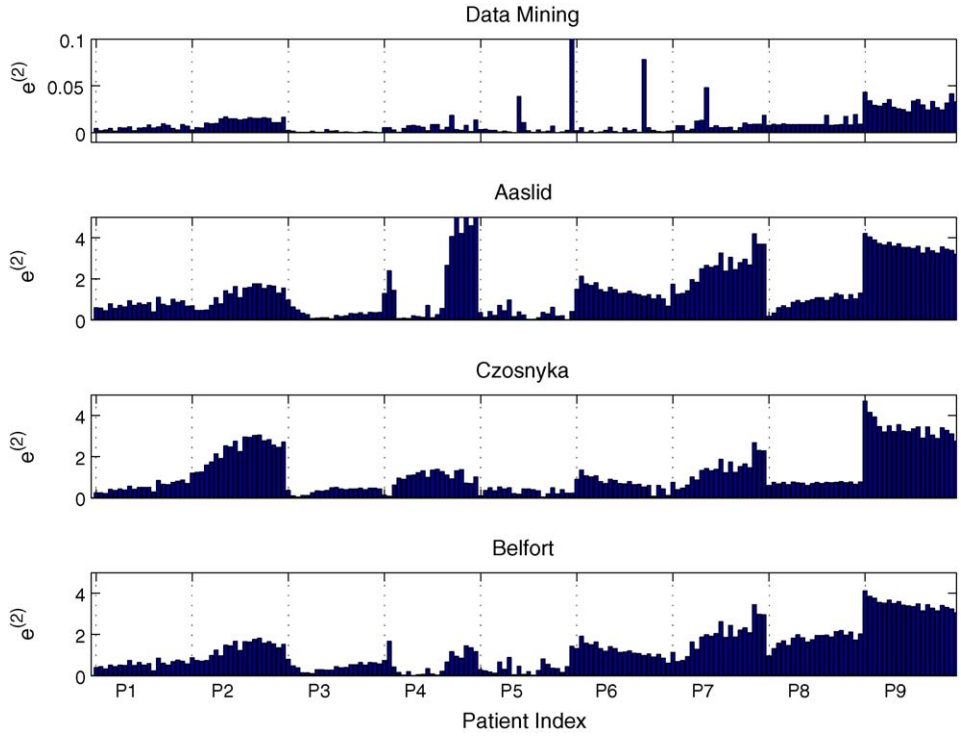

Fig. 6. Comparison of $e^{(2)}$ obtained using the proposed data mining approach to those obtained using three published NICP assessment methods.

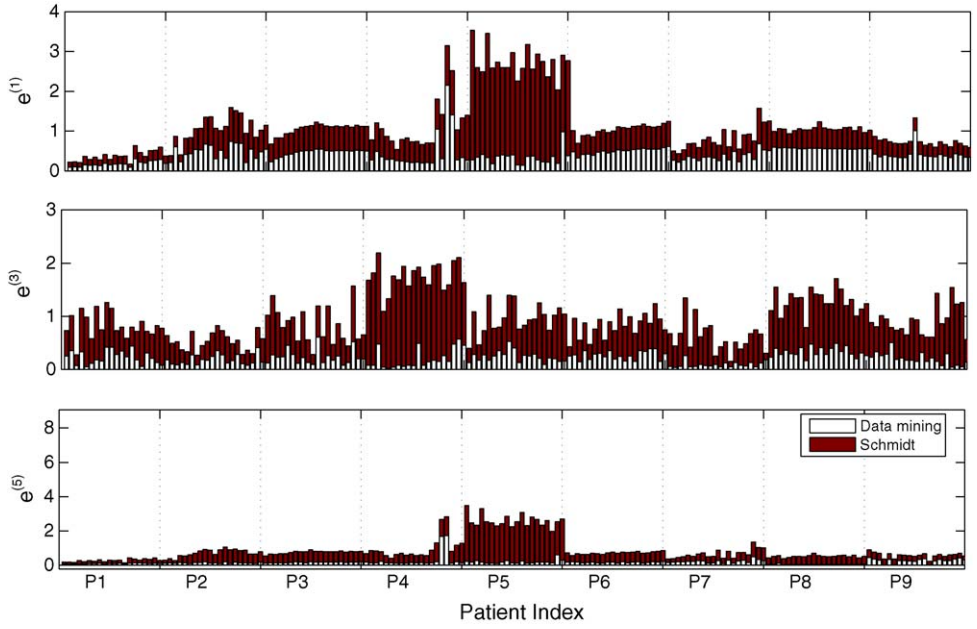

Fig. 7. Comparison of the proposed data mining approach, based on $e^{(1)}$, $e^{(3)}$ and $e^{(5)}$, with the published Schmidt method that can simulate ICP waveform. F_{slow} and robust query were used in the data mining approach.

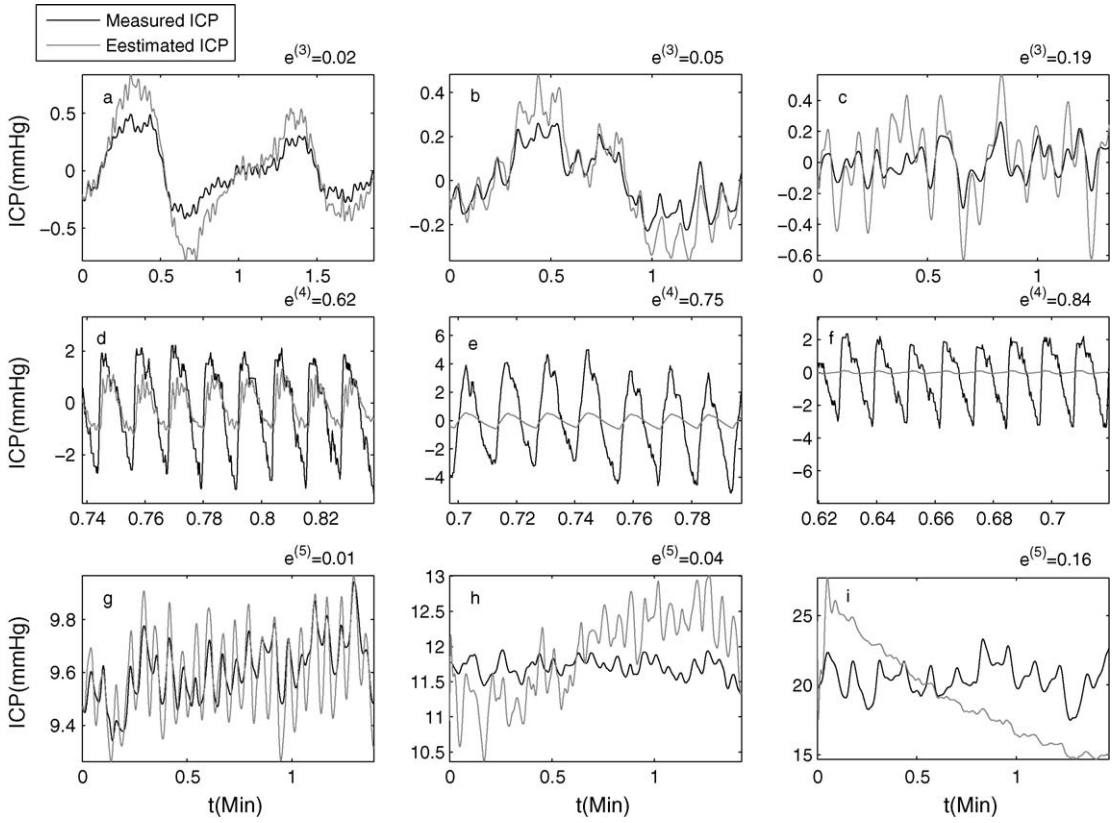

Fig. 8. A summary presentation of estimated ICP waveform based on different dissimilarity measures. Panels a, b, and c display the estimated and measured normalized ICP, panels d through f compare the pulsatile ICP while those of g through i show the slow-wave component of ICP. The left most column shows the database entries that achieved the smallest dissimilarity measure, the middle column shows those having dissimilarity measures close to the 10 percentile and the right most column shows those close to the 50 percentile.

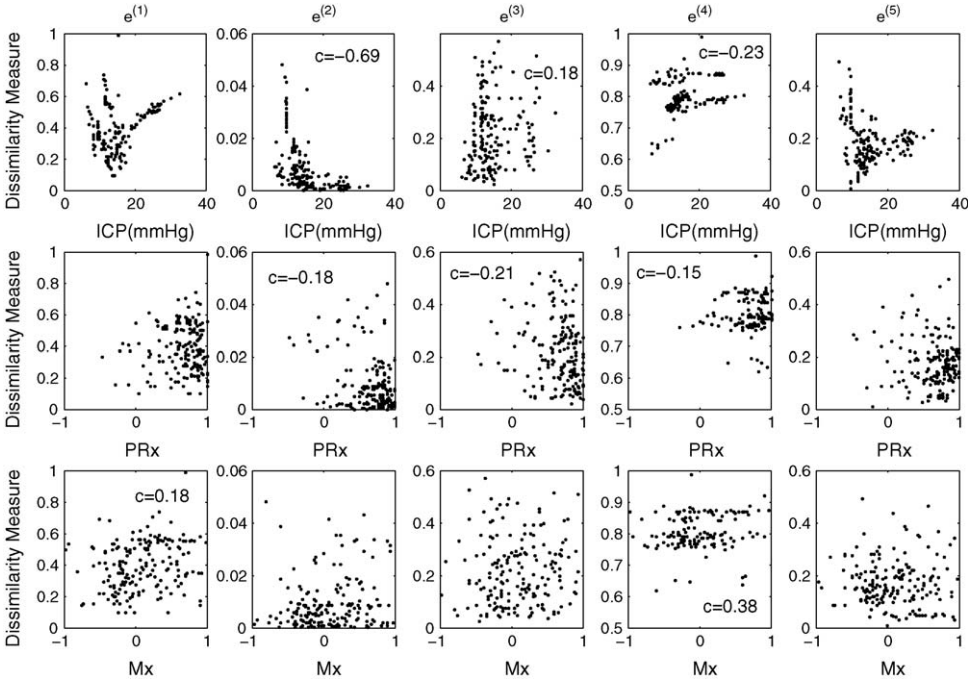

Fig. 9. Scatter plots of dissimilarity measures as a function of mean ICP (the first row), PRx (the second row) and Mx (the third row), respectively. PRx was calculated as running Pearson correlation coefficient between mean ICP and mean ABP; Mx was calculated as running Pearson correlation coefficient between mean CBFV and mean CPP.

can be seen from this figure that waveforms of estimated and measured normalized ICP are close to each other while the matching between those of pulsatile ICP component is poor even for the entry with smallest dissimilarity.

3.5. Factors influencing noninvasive ICP performance

The influence of mean ICP and pressure autoregulation status on the performance of ICP estimation was investigated. To characterize pressure autoregulation status, two existing measures including PRx and Mx were calculated. As described in [36,37], average ABP, CBFV, ICP and CPP were first computed using a running 10-s window. Then PRx and Mx were calculated as running Pearson correlation coefficient between consecutive averaged values of ABP and ICP, and CPP and CBFV, respectively. Thus each database entry is associated with a PRx and a Mx measure indicating their pressure autoregulation status. In addition, mean ICP of each database entry was also calculated. Results are presented in Fig. 9 as scatter plots where mean ICP, PRx and Mx are taken as x-axis and dissimilarity measures as y-axis. Spearman ρ was calculated for each scatter plot for investigating the correlation between x and y variables. Results were reported for scatter plots with significant non-zero ρ ($p < 0.05$). It can be seen from the figure that scatter plot between mean ICP and $e^{(1)}$ has a nonlinear shape with minimal dissimilarity achieved around 15 mmHg. This is the case for $e^{(5)}$ as well. Scatter plot between mean ICP and $e^{(2)}$ has a $1/x$ shape because of the mean ICP appears as the denominator in the equation for calculating $e^{(2)}$. Other scatter plots are less regular but some of them showed non-zero cross-correlation. Particularly, it is suggested that PRx and dissimilarity has a negative correlation while a positive correlation exists between Mx and dissimilarity.

4. Discussion

We have introduced a data mining framework for NICP assessment and demonstrated several implementation examples. In addition, a preliminary validation and evaluation of the proposed method was carried out based on a database containing nine patients with a strict leave-one-patient-out schema. These implementations may not be optimal but serve well for the purpose of illustrating the potential of the framework. The results obtained indicate that hemodynamic features that do not emphasize characteristics of each individual subject and the statistic query method that considers the imperfectness of the mapping function performed better for NICP simulation. The performance of the data mining method was shown to be superior to existing methods that use the same material for simulating ICP. However, considering that the signal database consisted of only nine patients' data, this result should be treated cautiously as a positive sign that motivates further evaluations with more clinical materials. Besides engaging more data in further evaluation, it is also important to continue improving the implementation of each component in the framework. Some of our thoughts in this direction will be discussed in sequel.

4.1. Mean ICP, PRx and Mx

The study of association between performance of the data-mining based NICP assessment and mean ICP, PRx and Mx indicated a preferable range of mean ICP where the NICP

assessment achieved minimal dissimilarity for $e^{(1)}$ and $e^{(5)}$. This region is between 12 and 15 mmHg, which is most populated. Consequently, more information is available for data entries having mean ICP within this range that leads to a better performance. PRx generally poses a small but significant negative correlation with the dissimilarity indicating that high correlation between ICP and ABP would lead to better performance of NICP assessment. This can be explained by the fact that ABP is one of input signals for estimating ICP. A better correlation between input and output would then lead to better estimate. On the other hand, Mx shows a small but significant positive correlation with the dissimilarity measure. This behavior is also expected because CBFV dynamics would reflect ICP dynamics as ICP fluctuations is a feedback input for regulating CBF if pressure autoregulation is intact. Therefore, small Mx indicating a better autoregulation would lead to small dissimilarity measure indicating better NICP assessment.

It has been demonstrated that incorporating measures, e.g., PRx and Mx of autoregulation status in the estimation process can improve the NICP assessment performance [21]. This would probably explain, at least partially, why the Schmidt's method [19] performed inferiorly to the proposed method because the distribution of average Mx of the nine patients in this study was wide ranging from −0.25 to 0.42. Therefore, the database is a mixture of recordings with preserved and impaired autoregulation that would negatively affect the performance of the Schmidt's method. While the enhanced Schmidt'method [21] essentially depends on two distinct signal databases separated by autoregulation status for gaining performance, the proposed method has a flexible structure to select an appropriate database entry on the fly and thus can avoid knowing each patient's autoregulation status as a prior.

4.2. Advantages of TCD based NICP assessment

Compared to other implementations of NICP assessment such as MR imaging, measuring displacement of skull and substituting inner ear pressure for ICP, the TCD based approaches are the most cost effective. Furthermore, given the fact that invasive ICP is still indispensable for the purpose of treating intracranial hypertension via diverting cerebrospinal fluid, the data mining approach originated in a neurosurgical environment can take its advantage by building up a properly sized database to conduct a NICP assessment for other services thus making a full use of the data collected while other data-independent approaches cannot directly use these data sets.

4.3. Comparison among existing methods

Various TCD based NICP assessment methods have been proposed since the first formation of the idea in 1985 [9]. The progress has been made in the sense that the original formula-based methods, which could only provide mean ICP, has evolved to the more sophisticated ones that can simulate ICP waveform [19,21]. The illustrated implementation of the framework is built upon those pioneering research, especially the idea of relying on the cerebral hemodynamic status to inversely infer ICP as advocated in the data driven approach proposed in [21]. However, as compared to the existing methods, the proposed framework has the main advantage of being flexible in many aspects. Firstly, the proposed framework does not attempt to build an ICP simulation model by pooling all training data. Instead, an intermediate minimum-dissimilarity-driven query was designed for discovering the most appropriate entry for building ICP simulation model. Therefore, the proposed method can enjoy the flexibility of accommodating a database of diversified entries. On the other hand, pooling all training data for building an ICP simulation model would require the homogeneity of the training database. Secondly, the framework is capable of responding to different requirements for noninvasively assessing various aspects of ICP by designing different dissimilarity measures and associated mapping functions. The existing methods lacks such flexibility. Thirdly, the framework is also versatile in incorporating different implementations of its various component blocks without much interference from each other. For example, the adoption of a new set of hemodynamic features does not require the change to the models chosen for ICP simulation. In this way, each block can be improved individually to enhance the overall system performance. Finally, the proposed method provides an estimate of the quality of NICP assessment, i.e., the estimated dissimilarity. Thus, a user can choose to disregard a NICP estimate if its associated dissimilarity exceeds certain limit. Such a feature is absent in the existing methods.

4.4. Future improvements to the implementation of the framework

Firstly, a proper extraction of hemodynamic features is of vital importance as in other pattern recognition applications. It has been found that hemodynamic features with less inter-patient separability are more appropriate for being used as hemodynamic features. Since LDA projection can be used to remove those patient-specific discriminant feature directions, it would be interesting to investigate whether or not this pre-processing of feature vectors can improve NICP assessment.

Secondly, it might also make more sense to use a nonlinear dynamic model instead of the linear one adopted in the present work for simulating ICP considering the inherent nonlinearity in the intracranial pressure dynamic system [38].

Thirdly, the current implementation of the database query returns only one database entry. An alternative way is to return a set of candidate entries and then fuse the estimated ICP from each of the models identified from them.

Furthermore, the availability of larger amount of data would lead to investigation of using a more versatile functional form to model the mapping function. Such choices may include variants of multiple-layer feedforward neural networks, radial basis networks and local linear fuzzy models. We consider that large amount of data is a prerequisite to adopt such complex models because of the problem of over-fitting.

One limitation in the present implementation is regarding the way a long recording was decomposed. A 30-min-long recording was arbitrarily broken into shorter database entries.

This schema may work for the data processed here since they were collected under a passive condition for a relatively short period during which patients state may not change. Therefore, there were no issues of nonstationarity. Indeed, one implicit assumption of the proposed method is that each database entry should be characterizable by a hemodynamic feature. Therefore, a segmentation procedure is necessary to break a long recording into shorter segments that stratify this assumption. One promising approach under investigation is to use a recursive identification of dynamics through a multiple model schema [39].

In summary, the present implementation serves mostly for an illustrating purpose and should open up future avenues to reach a better NICP assessment method.

Acknowledgements

The present work was funded by, in part, UCLA Brain Injury Research Center (BIRC), NINDS RO1 40122-01, and UCLA SPOTRIAS project.

References

[1] T. Ueno, R.E. Ballard, L.M. Shuer, J.H. Cantrell, W.T. Yost, A.R. Hargens, Noninvasive measurement of pulsatile intracranial pressure using ultrasound, Acta Neurochir. Suppl. (Wien) 71 (1998) 66–69.

[2] N.J. Alperin, S.H. Lee, F. Loth, P.B. Raksin, T. Lichtor, Mr-intracranial pressure (icp): a method to measure intracranial elastance and pressure noninvasively by means of mr imaging: baboon and human study, Radiology 217 (3) (2000) 877–885.

[3] P. Avan, B. Buki, B. Maat, M. Dordain, H.P. Wit, Middle ear influence on otoacoustic emissions. i: noninvasive investigation of the human transmission apparatus and comparison with model results, Hear. Res. 140 (1–2) (2000) 189–201.

[4] E. Thalen, H. Wit, H. Segenhout, F. Albers, Inner ear pressure changes following square wave intracranial or ear canal pressure manipulation in the same guinea pig, Eur. Arch. Otorhinolaryngol. 259 (4) (2002) 174–179.

[5] D. Michaeli, Z.H. Rappaport, Tissue resonance analysis; a novel method for noninvasive monitoring of intracranial pressure. technical note, J. Neurosurg. 96 (6) (2002) 1132–1137.

[6] A. Sidi, M.E. Mahla, Noninvasive monitoring of cerebral perfusion by transcranial doppler during fulminant hepatic failure and liver transplantation, Anesth. Analg. 80 (1) (1995) 194–200.

[7] K.L. Kaups, S.N. Parks, C.L. Morris, Intracranial pressure monitor placement by midlevel practitioners, J. Trauma 45 (5) (1998) 884–886.

[8] R.W. Sherman, R.A. Bowie, M.M. Henfrey, R.P. Mahajan, D. Bogod, Cerebral haemodynamics in pregnancy and pre-eclampsia as assessed by transcranial doppler ultrasonography, Br. J. Anaesth. 89 (5) (2002) 687–692.

[9] R. Aaslid, T. Lundar, K. Lindergaard, H. Nornes, Estimation of cerebral perfusion pressure from arterial blood pressure and transcranial doppler recordings, in: J.D. Miller, G.M. Teasdale, J.O. Rowan, S.L. Galbraith, A.D. Mendelow (Eds.), Proceedings of the Sixth International Symposium on Intracranial Pressure, Springer-Verlag, Glasgow, Scotland, 1985, pp. 226–229.

[10] M. Czosnyka, B.F. Matta, P. Smielewski, P.J. Kirkpatrick, J.D. Pickard, Cerebral perfusion pressure in head-injured patients: a noninvasive assessment using transcranial doppler ultrasonography, J. Neurosurg. 88 (5) (1998) 802–808.

[11] M.A. Belfort, C. Tooke-Miller, M. Varner, G. Saade, C. Grunewald, H. Nisell, J.A. Herd, Evaluation of a noninvasive transcranial doppler and blood pressure-based method for the assessment of cerebral perfusion pressure in pregnant women, Hypertens. Pregnancy 19 (3) (2000) 331–340.

[12] J. Klingelhofer, B. Conrad, R. Benecke, D. Sander, E. Markakis, Evaluation of intracranial pressure from transcranial doppler studies in cerebral disease, J. Neurol. 235 (3) (1988) 159–162.

[13] P.W. Hanlo, R.J. Peters, R.H. Gooskens, R.M. Heethaar, R.W. Keunen, A.C. van Huffelen, C.A. Tulleken, J. Willemse, Monitoring intracranial dynamics by transcranial doppler–a new doppler index: trans systolic time, Ultrasound Med. Biol. 21 (5) (1995) 613–621.

[14] M. Ursino, A mathematical study of human intracranial hydrodynamics. Part 1—the cerebrospinal fluid pulse pressure, Ann. Biomed. Eng. 16 (4) (1988) 379–401.

[15] M. Ursino, P. Di Giammarco, A mathematical model of the relationship between cerebral blood volume and intracranial pressure changes: the generation of plateau waves, Ann. Biomed. Eng. 19 (1) (1991) 15–42.

[16] M. Ursino, M. Iezzi, N. Stocchetti, Intracranial pressure dynamics in patients with acute brain damage: a critical analysis with the aid of a mathematical model, IEEE Trans. Biomed. Eng. 42 (6) (1995) 529–540.

[17] M. Ursino, C.A. Lodi, A simple mathematical model of the interaction between intracranial pressure and cerebral hemodynamics, J. Appl. Physiol. 82 (4) (1997) 1256–1269.

[18] T. Kailath, A.H. Sayed, B. Hassibi, Linear estimation, Prentice Hall information and system sciences series, Prentice Hall, Upper Saddle River, NJ, 2000.

[19] B. Schmidt, J. Klingelhöfer, J.J. Schwarze, D. Sander, I. Wittich, Noninvasive prediction of intracranial pressure curves using transcranial doppler ultrasonography and blood pressure curves, Stroke 28 (12) (1997) 2465–2472.

[20] B. Schmidt, M. Czosnyka, J.J. Schwarze, D. Sander, W. Gerstner, C.B. Lumenta, J. Klingelhofer, Evaluation of a method for noninvasive intracranial pressure assessment during infusion studies in patients with hydrocephalus, J. Neurosurg. 92 (5) (2000) 793–800.

[21] B. Schmidt, M. Czosnyka, A. Raabe, H. Yahya, J.J. Schwarze, D. Sackerer, D. Sander, J. Klingelhofer, Adaptive noninvasive assessment of intracranial pressure and cerebral autoregulation, Stroke 34 (1) (2003) 84–89.

[22] L. Ljung, System identification: theory for the user, in: Prentice Hall information and system sciences series, second ed., Prentice Hall PTR, Upper Saddle River, NJ, 1999.

[23] I.R. Piper, J.D. Miller, I.R. Whittle, A. Lawson, Automated time-averaged analysis of craniospinal compliance (short pulse response), Acta Neurochir. Suppl. (Wien) 51 (1990) 387–390.

[24] R.B. Panerai, R.P. White, H.S. Markus, D.H. Evans, Grading of cerebral dynamic autoregulation from spontaneous fluctuations in arterial blood pressure, Stroke 29 (11) (1998) 2341–2346.

[25] M. Oertel, D.F. Kelly, J.H. Lee, D.L. McArthur, T.C. Glenn, P. Vespa, W.J. Boscardin, D.A. Hovda, N.A. Martin, Efficacy of hyperventilation, blood pressure elevation, and metabolic suppression therapy in controlling intracranial pressure after head injury, J. Neurosurg. 97 (5) (2002) 1045–1053.

[26] R. Steinmeier, C. Bauhuf, U. Hubner, R.D. Bauer, R. Fahlbusch, R. Laumer, I. Bondar, Slow rhythmic oscillations of blood pressure, intracranial pressure, microcirculation, and cerebral oxygenation. dynamic interrelation and time course in humans, Stroke 27 (12) (1996) 2236–2243.

[27] R. Zhang, J.H. Zuckerman, B.D. Levine, Spontaneous fluctuations in cerebral blood flow: insights from extended-duration recordings in humans, Am. J. Physiol. Heart Circ. Physiol. 278 (6) (2000) H1848–H1855.

[28] J.J. Lemaire, T. Khalil, F. Cervenansky, G. Gindre, J.Y. Boire, J.E. Bazin, B. Irthum, J. Chazal, Slow pressure waves in the cranial enclosure, Acta Neurochir. (Wien) 144 (3) (2002) 243–254.

[29] R.B. Panerai, S.L. Dawson, J.F. Potter, Linear and nonlinear analysis of human dynamic cerebral autoregulation, Am. J. Physiol. 277 (3 Pt 2) (1999) H1089–H1099.

[30] H.K. Richards, M. Czosnyka, J.D. Pickard, Assessment of critical closing pressure in the cerebral circulation as a measure of cerebro-

vascular tone, Acta Neurochir. (Wien) 141 (11) (1999) 1221–1227, discussion 1226–7.

[31] X. Hu, V. Nenov, Multivariate ar modeling of electromyography for the classification of upper arm movements, Clin. Neurophysiol. 115 (6) (2004) 1276–1287.

[32] P.V. Overschee, B.L.R.D. Moor, Subspace Identification for Linear Systems: Theory, Implementation, Applications, Kluwer Academic Publishers, Boston, 1996.

[33] M. Verhaegen, P. Dewilde, Subspace model identification. 1. the output-error state-space model identification class of algorithms, Int. J. Control 56 (5) (1992) 1187–1210.

[34] L. W.E., Canonical variate analysis in identification, filtering and adaptive control, in: Proceedings of the 29th IEEE Conference Decision and Control, Honolulu, US, 1990, pp. 596–604.

[35] M.T. Hagan, H.B. Demuth, M.H. Beale, Neural Network Design, first ed., PWS Pub, Boston, 1996.

[36] M. Czosnyka, P. Smielewski, P. Kirkpatrick, D.K. Menon, J.D. Pickard, Monitoring of cerebral autoregulation in head-injured patients, Stroke 27 (10) (1996) 1829–1834.

[37] M. Czosnyka, P. Smielewski, P. Kirkpatrick, R.J. Laing, D. Menon, J.D. Pickard, Continuous assessment of the cerebral vasomotor reactivity in head injury, Neurosurgery 41 (1) (1997) 11–17 (discussion 17–9).

[38] X. Hu, V. Nenov, T.C. Glenn, L.A. Steiner, M. Czosnyka, N. Martin, M. Bergsneider, Nonlinear analysis of cerebral hemodynamical and intracranial pressure signals: Implication for a nonlinear measure of the autoregulation status, IEEE Trans. Biomed. Eng. 53 (2) (2006) 195–209.

[39] P. Andersson, Adaptive forgetting in recursive-identification through multiple models, Int. J. Control 42 (5) (1985) 1175–1193.

[40] G. Teasdale, B. Jennett, Assessment of coma and impaired consciousness. a practical scale, Lancet 2 (7872) (1974) 81–84.

[41] B. Jennett, M. Bond, Assessment of outcome after severe brain damage, Lancet 1 (7905) (1975) 480–484.